Scaling law in nonsequential double ionization by counter-rotating two-color circularly polarized laser fields

Mian Peng (彭 冕) and Lihua Bai (白丽华)*

Department of Physics, Shanghai University, Shanghai 200444, China
**Corresponding author: binger@shu.edu.cn*

Received May 21, 2020; accepted July 23, 2020; posted online September 23, 2020

Nonsequential double ionization (NSDI) of noble gas atoms in counter-rotating two-color circularly polarized (CRTC) laser fields is investigated. A scaling law is concluded by qualitatively and quantitatively comparing the momentum distributions of two electrons from NSDI in CRTC laser fields for different atoms with different parameters. The scaling law indicates that the momentum distributions from an atom driven by CRTC laser frequency ω_1, ω_2, and laser intensity I are the same as that from another atom irradiated by CRTC laser frequency $k\omega_1$, $k\omega_2$, and laser intensity k^3I. This study can provide an avenue in the research of two-color laser field ionization.

Keywords: scaling law; two-color laser; nonsequential double ionization.
doi: 10.3788/COL202018.110201.

The scaling law has wide applications in intense laser physics[1,2], which was firstly, to the best of our knowledge, derived when studying the photoelectron angular distribution of atoms irradiated by single-mode laser field[3]. Subsequent studies verified that the scaling law also exists in the few-cycle fields[4]. Then, the research also proved that there is a scaling law in the photoelectron spectra[5] and the high-order harmonics generated with photoionization[6]. It states that the three physical parameters of the single-electron dynamics process in an intense laser field, that is, the ponderomotive number $u_p = U_p/\hbar\omega$ (the ponderomotive energy U_p in units of laser photon energy), the binding number $\epsilon_b = E_b/\hbar\omega$ (the atomic binding energy E_b in units of laser photon energy), and the absorbed-photon number q during the ionization process remain unchanged after the scaling transfer. The main processes of photoionization, as well as many other electronic processes, are the same.

In recent years, two-color laser fields have been widely concerned[7–12]. The two-color laser field has been used to generate high-order circularly polarized harmonics[13–15]. Compared to the single-color laser fields, two-color laser fields can provide more parameters to control the electron motion in a two-dimensional plane. To form different combined electric fields, the polarization direction of two electric fields[16], the amplitude ratio of laser fields[17], and the relative phase[18] can be adjusted. Two-color circularly polarized laser fields can be further divided into counter-rotating and co-rotating circularly polarized lasers according to the relative rotation of two circularly polarized fields. The counter-rotating two-color circularly polarized (CRTC) laser field allows electrons to move in a two-dimensional plane and make a recollision, resulting in more nonsequential double ionization (NSDI) events. The co-rotating two-color circularly polarized laser field can hardly cause electrons to collide with each other[19], and the yield of NSDI is much less than that of the CRTC laser field. Studies have shown that in two-color co-rotating circularly polarized lasers, the momentum distribution of electrons exhibits a semi-circular arc structure[20], but, in the CRTC laser field, the momentum distribution of electrons exhibits a three-lobe structure. In the CRTC laser field, the yield of NSDI strongly depends on the amplitude ratio of the electric field, and, for Ar atoms, the yield of NSDI is the largest when the amplitude ratio is 1.5[21]. Very recently, studies have discussed that in the CRTC laser field with a frequency ratio of 1∶3, the NSDI events of O_2 molecules have been significantly increased[22].

In 2014, Dong *et al.*[23] verified the scaling law in strong-field NSDI using a full classical numerical simulation method with the help of a correlated momentum distribution[24]. In a single-color linearly polarized laser field, there is a scaling law for NSDI, but in a CRTC laser field, is there also a scaling law for NSDI?

In this Letter, we use the two-dimensional full classical numerical method to investigate the NSDI of Ar atoms in the CRTC laser field. Numerical simulation results show that the momentum distribution of Ar atoms in the polarization plane has a clear three-lobed structure and presents a triangular distribution, which is consistent with previous experiments and simulations[25,26]. We also establish the scaling law of NSDI in the CRTC laser field and calculate the momentum distribution of different target atoms by changing the laser intensity and laser frequency. The results of the simulation calculations show the scaling law, which means that the scaling law is not only applicable to the single-electron case and the single-color laser field two-electron case, but also the two-electron case in the CRTC laser field. The scaling coefficient k is also different from the previous discussion[23], where k equals the ratio of the second ionization potentials of two atoms.

Because the full quantum numerical simulation method is to solve the time-dependent Schrödinger equation[27], it demands a huge computational condition for

multi-electronic systems, and the full classical numerical simulation method[28,29] is also very effective in the study of electron dynamics. It numerically solves the time-dependent Newton's equation of motion. It can record the trajectory of each electron from the beginning to the end of the pulse so that the momentum process of the two electrons can be back-analyzed, and the amount of calculation is relatively easy. Therefore, in recent years, this method has been widely used in the research field of intense laser field electron dynamics[30]. The full classical method to study the scaling law of NSDI for noble gas atoms in the CRTC laser field is also used in this Letter.

The Hamiltonian of a two-active-electron atom without an electric field can be written as (in atomic units)

$$H_e = \sum_{i=1,2}\left(\frac{\mathbf{p}_i^2}{2} - \frac{2}{\sqrt{\mathbf{r}_i^2 + a^2}}\right) + \frac{1}{\sqrt{(\mathbf{r}_1 - \mathbf{r}_2)^2 + b^2}}, \quad (1)$$

where it is usually the sum of the first ionization potential and the second ionization potential, and $\mathbf{r}_i$ and $\mathbf{p}_i$ represent the position and momentum ($i = 1, 2$) of the electron, respectively. The potential $-2/\sqrt{\mathbf{r}_i^2 + a^2}$ represents the ion–electron Coulomb interactions, and the potential $1/\sqrt{(\mathbf{r}_1 - \mathbf{r}_2)^2 + b^2}$ represents the electron–electron Coulomb interactions. Here, a and b are called softening parameters; a is introduced here to avoid autoionization, and b is included primarily for numerical stability. In our calculations, a and b have different values for different atoms. The specific parameters are shown in Table 1.

The nucleus is at the origin of the coordinates, and the Hamiltonian of the two electrons in the laser field is given by

$$H = H_e + (\mathbf{r}_1 + \mathbf{r}_2) \cdot \mathbf{E}(t), \quad (2)$$

where $\mathbf{E}(t) = \mathbf{E}_x(t) + \mathbf{E}_y(t)$ is the electric field of the CRTC laser pulse. It can be written as

$$E_x(t) = \frac{E_0}{\sqrt{2}(1+\gamma_E)} f(t)[\cos(\omega_1 t)] + \frac{\gamma_E E_0}{\sqrt{2}(1+\gamma_E)} f(t)[\cos(\omega_2 t)], \quad (3)$$

Table 1. Values of Softening Parameters a, b and Hamiltonian of a Two-Electron Atom Used in This Letter

Atoms	Hamiltonian (a.u.)	a (a.u.)	b (a.u.)
He	−2.9035	0.825	0.05
Ne	−2.2980	1.000	0.10
Ar	−1.5946	1.500	0.05

$$E_y(t) = \frac{E_0}{\sqrt{2}(1+\gamma_E)} f(t)[\sin(\omega_1 t)] - \frac{\gamma_E E_0}{\sqrt{2}(1+\gamma_E)} f(t)[\sin(\omega_2 t)], \quad (4)$$

where E_0 is the combined electric field amplitude. ω_1 and ω_2 are the fundamental laser frequency and second harmonic laser frequency of two laser fields, respectively. In this Letter, $\omega_1 = 0.0576$ a.u. (corresponding wavelength is 790 nm) and $\omega_2 = 0.115$ a.u. (corresponding wavelength is 395 nm). γ_E is the electric field amplitude ratio of the second harmonic laser pulse and the fundamental laser pulse. $f(t) = \sin^2(\pi t/NT)$ is the pulse envelope function, where N is the number of optical cycles, and T is the period of the 790 nm laser field. In our simulation, N is equal to 10, and γ_E is equal to 1, which means that the laser intensities of two laser pulses are the same. In our calculations, the electric field shows a trefoil pattern, and the negative vector potential traces out a triangle structure. The motion of two electrons is governed by Newton's equations of motion as the following:

$$\frac{\mathrm{d}\mathbf{r}_i}{\mathrm{d}t} = \frac{\partial H}{\partial \mathbf{p}_i}, \quad \frac{\mathrm{d}\mathbf{p}_i}{\mathrm{d}t} = -\frac{\partial H}{\partial \mathbf{r}_i}. \quad (5)$$

This equation can be solved by using the standard fourth to fifth Runge–Kutta algorithm. The initial position and momentum distribution of the two electrons satisfy the Gaussian random distribution that ensures that the total kinetic energy is positive. Then, the electrons are allowed to evolve freely a long time (100 a.u.), where the position and momentum distribution of the electrons are stable. After a stable initial ensemble is obtained, the laser field is added, and all electrons begin to evolve under the collective effect of the Coulomb potential and electric field until the end of the pulse. When the total energy of both electrons is greater than zero at the end of the pulse, it is recorded as a double ionization event.

We explored the scaling law of different noble gas atoms in the CRTC laser field through a scaling method. Here, we mainly study the electron momentum distribution of NSDI of three atoms for Ar, Ne, and He in the CRTC laser field. According to the scaling law, the photoelectron momentum distribution is determined by the ponderomotive parameter $u_p = U_p/\hbar\omega$, the binding number $\epsilon_b = E_b/\hbar\omega$, and the absorbed-photon number q. In previous research, when studying the angular distribution of photoelectrons in the above-threshold ionization[31], it was found that the angular distribution of photoelectrons from atoms with binding energy E_b irradiated by a linearly polarized laser pulse with a laser frequency ω and laser intensity I and atoms with binding energy kE_b irradiated by the linearly polarized laser pulse with a laser frequency $k\omega$ and laser intensity $k^3 I$ has a similar structure, which indicates that there is a scaling law in the process of single ionization.

In this Letter, we mainly study the momentum distribution spectrum obtained by the CRTC laser on noble gas atoms. In the double ionization process, energy conservation is

$$E_{k1} + E_{k2} = N\omega - (I_{p1} + I_{p2}) - 2u_p\omega, \tag{6}$$

where E_{k1} and E_{k2} denote the final kinetic energy of the first and the second photoelectron, respectively; N denotes the number of photons absorbed during double ionization; I_{pi} denotes the ith ionization potential of the atom. It can be known from Eq. (6) that to ensure the momentum distributions to show a similarity for different atoms, it is necessary to keep u_p unchanged. The u_p is the individual and total ponderomotive energies divided by the photon energies. We define the average frequency $\bar{\omega}$[32–34], and the scaling can be reduced to the average frequency $\bar{\omega} = (\omega_1 + \omega_2)/2$ and one ponderomotive energy. The ponderomotive parameter is $u_p = I/4\bar{\omega}^3$. Then, increase $\bar{\omega}$ by k times, and increase I by k^3 times, so we have

$$u_p = Ik^3/4\bar{\omega}^3k^3 = I/4\bar{\omega}^3, \tag{7}$$

which shows that u_p does not change. When increasing I by k^2 times, the ponderomotive parameter is $u_p = I/4k\bar{\omega}^3$, which indicates that u_p has changed. So, u_p, which scales as k^3, is more useful.

Subsequently, we need to determine the scaling ratio k. In the research of Ref. [23], three k values were determined, which are $k_1 = I_{p1}/I'_{p1}$, $k_2 = (I_{p1} + I_{p2})/(I'_{p1} + I'_{p2})$, and $k_3 = I_{p2}/I'_{p2}$, where I'_{p1} and I'_{p2} are the first and second ionization potentials of another atom, respectively. When $k = k_3$, the momentum distribution spectra obtained by different atoms have a similar structure. However, in our research, taking the above three k values do not yield an effective similar structure, which may be due to the two-color laser interaction on the atom, and it has a more complex and changeable electrodynamic process. We consider that the two-color field has greater ponderomotive energy than the single-color field, so we preferentially consider the value of k in the two-color field to be greater than the ratio of the second ionization energy. Then, we accumulate the second ionization energy ratio by 0.005 as the value of k. We take multiple test values and obtain the momentum distribution through many calculations. We compared the similarity of the momentum distribution spectrum and the momentum distribution probabilities (MDPs) and finally determined the optimal k value.

The momentum distributions of NSDI for Ar atoms are shown in Fig. 1. In calculation, the wavelengths of CRTC are chosen as $\lambda_1 = 790\,\text{nm}$ and $\lambda_2 = 395\,\text{nm}$. The laser intensities are chosen as $I_0 = 2 \times 10^{14}\,\text{W/cm}^2$ [Fig. 1(a)] and $4 \times 10^{14}\,\text{W/cm}^2$ [Fig. 1(b)], respectively. The red and yellow areas in the figure are the low-energy structure distribution, and we can see that the distribution of the low-energy structure is different for different laser intensities. When the laser intensity is at $2 \times 10^{14}\,\text{W/cm}^2$, the low-energy structure is from the fourth quadrant to the third quadrant, as shown in Fig. 1(a). For Fig. 1(b), the momentum distribution has a low-energy structure like the number "7". The low-energy structure spans the third quadrant and the second quadrant but is mainly in the second quadrant.

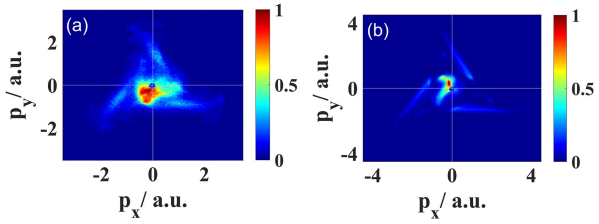

Fig. 1. Momentum distributions of two electrons at different laser intensities for an Ar atom irradiated by CRTC laser wavelengths of 790 nm and 395 nm. For (a) and (b), the laser intensity is chosen as $I_0 = 2 \times 10^{14}\,\text{W/cm}^2$ and $4 \times 10^{14}\,\text{W/cm}^2$, respectively. The two colors are of equal intensity.

In order to verify the scaling law, the NSDI momentum distribution is calculated for Ne and He. In the calculation for Ne atoms, we take $k = 1.587$ and $k = 2.154$ for He atoms.

Figure 2 shows the momentum distribution of Ne atoms and He atoms in laser pulses with varying laser frequencies and laser intensities. Figures 2(a)–2(c) show

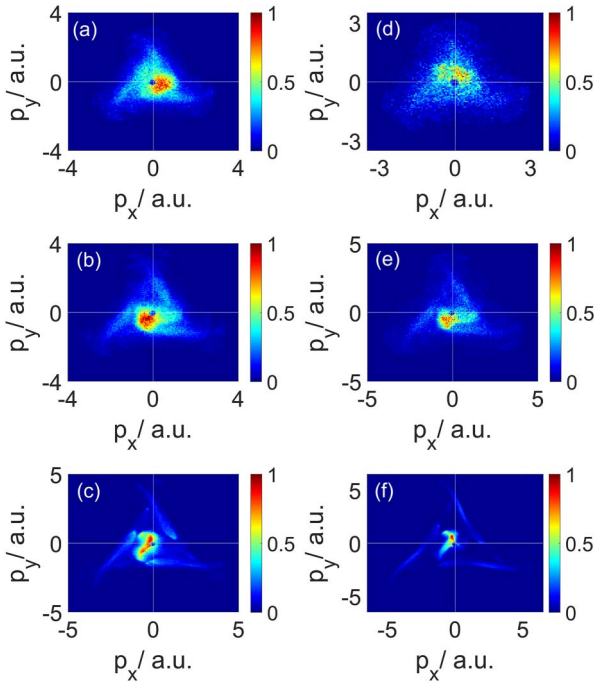

Fig. 2. Momentum distributions of two electrons from a Ne atom irradiated by CRTC laser wavelengths of 498 nm and 249 nm, with laser intensities (a) $5.04 \times 10^{14}\,\text{W/cm}^2$, (b) $7.99 \times 10^{14}\,\text{W/cm}^2$, and (c) $1.27 \times 10^{15}\,\text{W/cm}^2$, respectively. The He atoms are irradiated by CRTC laser wavelengths of 366 nm and 183 nm, with laser intensities (d) $9.28 \times 10^{14}\,\text{W/cm}^2$, (e) $1.99 \times 10^{15}\,\text{W/cm}^2$, and (f) $4.31 \times 10^{15}\,\text{W/cm}^2$, respectively. The two colors are of equal intensity.

the momentum distribution of Ne atoms driven by laser wavelengths λ_1/k, λ_2/k and laser intensities k^2, k^3, and k^4 times of I_0, respectively. At the laser intensity of $5.04 \times 10^{14}\,\mathrm{W/cm^2}$ ($k^2 I_0$), the low-energy structure in the calculated momentum distribution takes over four quadrants, which are highlighted with the accumulation of more electrons. This is different from the momentum feature shown in Fig. 1(a). The momentum distribution calculated at laser intensity $1.27 \times 10^{15}\,\mathrm{W/cm^2}$ ($k^4 I_0$) also differs much from Fig. 1(a). The electrons distribute dispersively in the second and the third quadrants, and thus the bright areas are large. These discrepancies disappear when the laser intensity is set as $7.99 \times 10^{14}\,\mathrm{W/cm^2}$ ($k^3 I_0$), and its momentum distribution [Fig. 2(b)] is very similar to Fig. 1(a). It is found that the low-energy structure distributes mainly in the third quadrant of Fig. 2(b), which is the same as that in Fig. 1(a). But, the low-energy structure in Figs. 2(a) and 2(c) is different from Fig. 1(a). So, there is a scaling law for the Ne atoms. Figures 2(d)–2(f) show the momentum distribution spectrum of He atoms for laser wavelengths of 366 nm and 183 nm. The laser intensities are chosen as k^2, k^3, and k^4 times of I_0, respectively. According to the features of the low-energy structure in Fig. 1(a), it is easy to find that the momentum distribution in Fig. 2(e), which is the one most similar to the referential momentum distribution, while the momentum distributions of the low-energy structure in Figs. 2(d) and 2(f) differ greatly from the referential one. Hence, we judge that the momentum distribution calculated at laser intensity $k^3 I_0$ is the one most like the referential one. This comparison indicates that the scaling law holds for the He atom.

The above simulation results prove that the scaling law does exist in our calculation. The theoretical explanation produced by the scaling law is that although the intensity and angular frequency of the laser field are changed, the ponderomotive parameter of the laser is not changed; so, under two laser fields, the photoelectrons of different atoms will have the same dynamic process.

Subsequently, we calculate the momentum distributions of NSDI for Ne and He atoms with different laser intensities when the laser wavelength and the scaling ratio k are unchanged, as shown in Fig. 3. Figures 3(a)–3(c) are the momentum distribution spectra of Ne atoms at CRTC laser intensities $k^2 I_0$, $k^3 I_0$, and $k^4 I_0$, respectively. Figures 3(d)–3(f) are for that of He atoms. It shows that Figs. 3(b) and 3(e) have low-energy structures like the number "7". They are very similar to low-energy structures in Fig. 1(b). However, the low-energy structure is not the same as that in other figures. This comparison indicates that the scaling law holds for higher laser intensity situations. The intensities of the two lasers are different, resulting in different recollision times, subsequently inducing different low-energy structures. In the scaling law, although we change the laser intensity, the ponderomotive parameters are unchanged, and different atoms have the same recollision time, so they have the same low-energy structure.

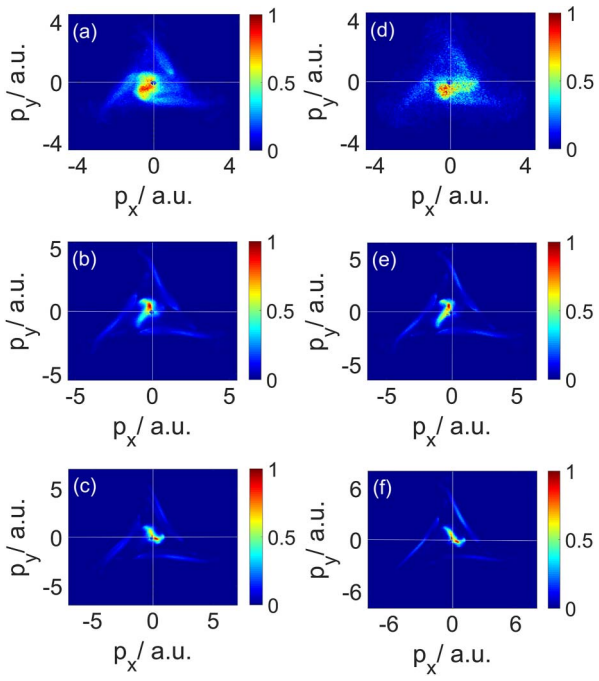

Fig. 3. Momentum distribution of two electrons from a Ne atom irradiated by CRTC laser wavelengths of 498 nm and 249 nm, with laser intensities (a) $1.01 \times 10^{15}\,\mathrm{W/cm^2}$, (b) $1.59 \times 10^{15}\,\mathrm{W/cm^2}$, and (c) $2.54 \times 10^{15}\,\mathrm{W/cm^2}$, respectively. The He atom irradiated by CRTC laser wavelengths of 366 nm and 183 nm, with laser intensities (d) $1.86 \times 10^{15}\,\mathrm{W/cm^2}$, (e) $3.99 \times 10^{15}\,\mathrm{W/cm^2}$, and (f) $8.62 \times 10^{15}\,\mathrm{W/cm^2}$. The two colors are of equal intensity.

To quantitatively analyze the momentum distribution of the ionized electrons, we calculate the ratio of the momentum distribution in different quadrants. Figure 4 depicts MDPs of ionized electrons in different quadrants.

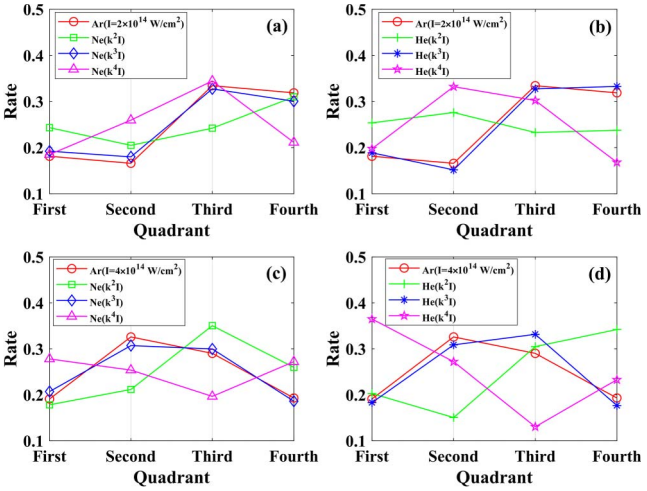

Fig. 4. MDP in four quadrants for Ar atoms, Ne atoms, and He atoms. (a) and (c) show the MDP of Ar atoms at CRTC laser intensities $I_0 = 2 \times 10^{14}\,\mathrm{W/cm^2}$ and $4 \times 10^{14}\,\mathrm{W/cm^2}$, respectively, compared with Ne atoms at laser intensities $k^2 I_0$, $k^3 I_0$, and $k^4 I_0$, respectively. (b) and (d) show the MDP of He atoms with the same parameters as (a).

In Fig. 4(a), the red line represents the MDP of Ar atoms at CRTC laser wavelengths of 790 nm and 395 nm, with laser intensity of $2 \times 10^{14}\,\mathrm{W/cm^2}$, and the green, blue, and pink lines represent the MDP of Ne atoms at CRTC laser wavelengths of 498 nm and 249 nm, with laser intensities of $5.04 \times 10^{14}\,\mathrm{W/cm^2}$, $7.99 \times 10^{14}\,\mathrm{W/cm^2}$, and $1.27 \times 10^{15}\,\mathrm{W/cm^2}$, respectively. The red line in Fig. 4(b) is the same as that in Fig. 4(a), and the green, blue, and pink lines represent the MDP of He atoms at CRTC laser wavelengths of 366 nm and 183 nm, with laser intensities of $5.04 \times 10^{14}\,\mathrm{W/cm^2}$, $7.99 \times 10^{14}\,\mathrm{W/cm^2}$, and $1.27 \times 10^{15}\,\mathrm{W/cm^2}$, respectively. Figures 4(c) and 4(d) show the MDP when I_0 is changed to $4 \times 10^{14}\,\mathrm{W/cm^2}$. In each panel, the blue line is closer to the red line, which means that they have similar MDPs in different quadrants. The above phenomenon indicates that the target atom and the original atom have the same dynamic process after changing the laser parameters according to the scaling law. This qualitatively proves the existence of a scaling law in the CRTC laser field.

Finally, we test the scaling law for the generality of the laser frequency of the laser field. Figures 5(a) and 5(b) show the momentum distribution of Ne atoms and He atoms in the CRTC laser field of intensity $k^3 I_0$. The laser wavelengths are chosen as λ_1, λ_2 [Fig. 5(a)] and λ_1/k^2, λ_2/k^2 [Fig. 5(b)], respectively. We compare the momentum distribution of the Ar atom at the laser intensity of $2 \times 10^{14}\,\mathrm{W/cm^2}$ and laser wavelengths of 790 nm and 395 nm [Fig. 1(a)] with the momentum distribution for the Ne atom [Figs. 5(a) and 5(b)]. The dissimilarity in the momentum distribution shows that the optimal laser wavelength is λ/k, i.e., the frequency is $k\omega$. Figures 5(c) and 5(d) show the momentum distribution of He atoms at laser intensity $k^3 I_0$. The laser wavelengths are chosen as λ_1, λ_2 [Fig. 5(c)] and $\lambda_1/k^2, \lambda_2/k^2$ [Fig. 5(d)], respectively.

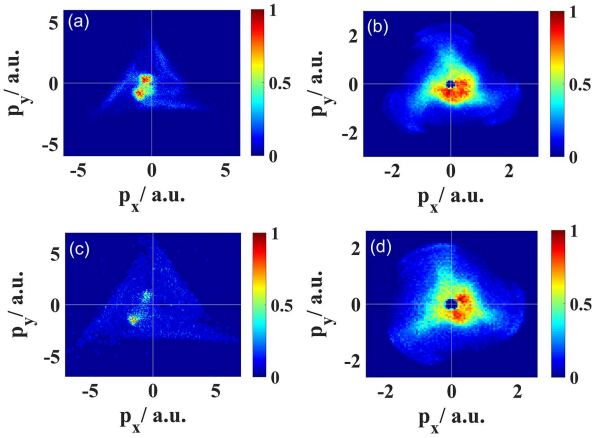

Fig. 5. Momentum distribution of two electrons from a Ne atom irradiated by CRTC laser intensity of $7.99 \times 10^{14}\,\mathrm{W/cm^2}$, with laser wavelengths of (a) 790 nm and 395 nm, (b) 314 nm and 157 nm, respectively. (c) and (d) show the momentum distribution of two electrons from a He atom irradiated by CRTC laser intensity of $1.99 \times 10^{15}\,\mathrm{W/cm^2}$, with laser wavelengths of (c) 790 nm and 395 nm, (d) 170 nm and 85 nm, respectively.

These momentum distributions differ greatly from the referential one [Fig. 1(b)]. Wavelengths of the two lasers are different, resulting in different recollision times, subsequently inducing different low-energy structures. In the scaling law, although we change the laser wavelength, the ponderomotive parameters are unchanged, and different atoms have the same recollision time, so they have the same low-energy structure. This illustrates that the best laser frequency conversion is ω to $k\omega$.

Compared with the case of the single-color laser, the value of k we give in the scaling law of the two-color field is obtained by summing up the results of numerical calculations. For different atoms, the value of k is different. Our present scale parameter k is not a general formula applicable to all noble gas atoms. For atoms that we have not calculated, such as Xe atoms and Kr atoms, we need to calculate the value of k separately. Our calculation results also provide a direction for finding the value of k for other noble gas atoms and indicate that the value of k is greater than the ratio of the second ionization energy. The value of the k factor given by our calculation is general for the electric field ratio of the two-color laser field. When we change the electric field ratio, the value of k is still the same, which shows that the value of k taken by our method is very effective.

In conclusion, we have investigated the momentum distribution spectrum of NSDI for the three noble gas atoms Ar, Ne, and He in CRTC laser fields. Through qualitatively and quantitatively comparative research, we propose the scaling law of CRTC laser fields. When we change the laser intensity and laser frequency of the laser pulse according to the scaling law at the same time, the ponderomotive parameters remain unchanged, and most of the electron dynamics processes and ionization processes will remain the same. Different atoms have the same momentum distribution in different laser fields. Because the ponderomotive parameters of a two-color laser field are constant, the electrons' recollision times are the same, subsequently inducing the same low-energy structures. The conclusion of the study can provide an avenue for the research of two-color laser field ionization.

This work was supported by the Natural Science Foundation of Shanghai (No. 18ZR1413600).

References

1. A. Gordon and F. Kartner, Opt. Express **13**, 2941 (2005).
2. X. Chen, Y. Wu, and J. Zhang, Phys. Rev. A **95**, 013402 (2017).
3. D. S. Guo, J. Zhang, Z. Xu, X. Li, P. Fu, and R. R. Freeman, Phys. Rev. A **68**, 043404 (2003).
4. J. Zhang, L. Bai, S. Gong, Z. Xu, and D.-S. Guo, Opt. Express **15**, 7261 (2007).
5. H. Ye, Y. Wu, J. Zhang, and D.-S. Guo, Opt. Express **19**, 20849 (2011).
6. Y. Wu, H. Ye, C. Shao, and J. Zhang, Chin. Phys. B **21**, 024210 (2012).
7. C. A. Mancuso, K. M. Dorney, D. D. Hickstein, J. L. Chaloupka, J. L. Ellis, F. J. Dollar, R. Knut, P. Grychtol, D. Zusin, C. Gentry,

M. Gopalakrishnan, H. C. Kapteyn, and M. M. Murnane, Phys. Rev. Lett. **117**, 133201 (2016).
8. K. Lin, X. Jia, Z. Yu, F. He, J. Ma, H. Li, X. Gong, Q. Song, Q. Ji, W. Zhang, H. Li, P. Lu, H. Zeng, J. Chen, and J. Wu, Phys. Rev. Lett. **119**, 203202 (2017).
9. C. Jin and C. D. Lin, Photon. Res. **6**, 434 (2018).
10. L. He, G. Yuan, K. Wang, W. Hua, C. Yu, and C. Jin, Photon. Res. **7**, 1407 (2019).
11. J. Liu, W. Li, J. Liu, W. Wang, R. Qi, Z. Zhang, C. Yu, Z. Qin, M. Fang, K. Feng, Y. Wu, C. Wang, and R. Li, Chin. Opt. Lett. **16**, 071202 (2018).
12. L. G. Huang, H. Takabe, and T. E. Cowan, High Power Laser Sci. Eng. **7**, e22 (2019).
13. W. Becker, B. N. Chichkov, and B. Wellegehausen, Phys. Rev. A **60**, 1721 (1999).
14. A. Fleischer, O. Kfir, T. Diskin, P. Sidorenko, and O. Cohen, Nat. Photon. **8**, 543 (2014).
15. O. Kfir, P. Grychtol, E. Turgut, R. Knut, D. Zusin, D. Popmintchev, T. Popmintchev, H. Nembach, J. M. Shaw, A. Fleischer, H. Kapteyn, M. Murnane, and O. Cohen, Nat. Photon. **9**, 99 (2015).
16. C. A. Mancuso, D. D. Hickstein, K. M. Dorney, J. L. Ellis, E. Hasović, R. Knut, P. Grychtol, C. Gentry, M. Gopalakrishnan, D. Zusin, F. J. Dollar, X.-M. Tong, D. B. Milošević, W. Becker, H. C. Kapteyn, and M. M. Murnane, Phys. Rev. A **93**, 053406 (2016).
17. X. Ma, Y. Zhou, Y. Chen, M. Li, Y. Li, Q. Zhang, and P. Lu, Opt. Express **27**, 1825 (2019).
18. M. Han, P. Ge, Y. Shao, Q. Gong, and Y. Liu, Phys. Rev. Lett. **120**, 073202 (2018).
19. C. A. Mancuso, D. D. Hickstein, P. Grychtol, R. Knut, O. Kfir, X. Tong, F. Dollar, D. Zusin, M. Gopalakrishnan, C. Gentry, E. Turgut, J. L. Ellis, M. Chen, A. Fleischer, O. Cohen, H. C. Kapteyn, and M. M. Murnane, Phys. Rev. A **91**, 031402 (2015).
20. C. Huang, M. Zhong, and Z. Wu, Opt. Express **27**, 7616 (2019).
21. S. Eckart, M. Richter, M. Kunitski, A. Hartung, J. Rist, K. Henrichs, N. Schlott, H. Kang, T. Bauer, H. Sann, L. P. H. Schmidt, M. Schöffler, T. Jahnke, and R. Dörner, Phys. Rev. Lett. **117**, 133202 (2016).
22. B. Li, X. Yang, X. Ren, and J. Zhang, Opt. Express **27**, 32700 (2019).
23. S. Dong, Z. Zhang, L. Bai, and J. Zhang, Phys. Rev. A **92**, 033409 (2015).
24. Z. Zhang, L. Bai, and J. Zhang, Phys. Rev. A **90**, 023410 (2014).
25. D. Wu, X. He, W. Yu, and S. Fritzsche, High Power Laser Sci. Eng. **6**, e50 (2018).
26. C. Huang, M. Zhong, and Z. Wu, Opt. Express **26**, 26045 (2018).
27. K. J. Yuan, S. Chelkowski, and A. D. Bandrauk, Phys. Rev. A **93**, 053425 (2016).
28. F. Feng and L. Bai, Chin. Opt. Lett. **16**, 063201 (2018).
29. S. L. Haan, L. Breen, A. Karim, and J. H. Eberly, Phys. Rev. Lett. **97**, 103008 (2006).
30. Y. Liu, L. Fu, D. Ye, J. Liu, M. Li, C. Wu, Q. Gong, R. Moshammer, and J. Ullrich, Phys. Rev. Lett. **112**, 013003 (2014).
31. J. Liang, R. Zhang, X. Ma, Y. Zhou, and P. Lu, Chin. Opt. Lett. **16**, 040202 (2018).
32. A. D. Bandrauk and H. Lu, Phys. Rev. A **68**, 043408 (2003).
33. D. M. Reich and L. B. Madsen, Phys. Rev. A **93**, 043411 (2016).
34. A. D. Bandrauk, J. Guo, and K. J. Yuan, J. Opt. **19**, 124016 (2017).